Electronic State Interferences in Resonant X-Ray Emission after *K*-Shell Excitation in HCl

M. Kavčič, M. Žitnik, K. Bučar, and A. Mihelič
Jožef Stefan Institute, Post Office Box 3000, SI-1001 Ljubljana, Slovenia

S. Carniato, L. Journel, R. Guillemin, and M. Simon
UPMC Univ Paris 06, UMR 7614, Laboratoire de Chimie Physique Matière et Rayonnement, F-75005 Paris, France
CNRS, UMR 7614, Laboratoire de Chimie Physique Matière et Rayonnement, F-75005 Paris, France
(Received 7 July 2010; published 10 September 2010)

We have measured a series of high-resolution x-ray spectra emitted upon resonant photoexcitation of HCl. The photon energy was tuned across the dissociative $1s \rightarrow 6\sigma^*$ resonance and the Rydberg states converging to the Cl $1s^{-1}$ threshold, and inelastic photon scattering was observed in the region of *KL* emission lines. Excellent agreement is found between fully *ab initio* calculated and measured spectra if interferences between different excitation-emission paths are taken into account. The effect of electronic state interferences is enhanced due to dynamical broadening of the $6\sigma^*$ resonance in HCl.

DOI: 10.1103/PhysRevLett.105.113004 PACS numbers: 33.80.−b, 33.20.Rm

Bound atomic or molecular states are coherently excited if they overlap in energy, and the overlap can be considerable when the lifetime broadening Γ is larger or comparable to the energy difference between excited states. If a group of coherently excited states decays to the same final state, interference effects may be observed in the corresponding decay channel. This is manifested, for example, by quantum beats showing up in time dependent yield of decay products [1], or by modulation of photoelectron angular distribution due to overlap of spin-orbit multiplet terms [2]. A well-known example in molecular physics is provided by lifetime-vibrational interferences. Because of the relatively short lifetime of core-excited states, linewidths are of the same magnitude as vibrational level spacings, and there is a nonnegligible probability that the same final state is populated through different coherently excited intermediate vibronic states. In order to explain the observed Auger and x-ray spectra, excitation and decay cannot be treated as independent processes, and a one-step formalism is required. The first observations of lifetime-vibrational interferences were made using high-energy electron probes, but due to broadband excitation, the interferences were largely obscured by the predominant amplitude of the lowest vibrational mode [3,4]. The subsequent spectroscopic studies of resonant Auger or resonant x-ray emission employed energy selective photoexcitation to disentangle lifetime-vibrational interference effects on small diatomic molecules (see for instance [5–7]).

The theoretical description of lifetime-vibrational interferences has been generalized to include interferences resulting from coherent excitation of different overlapping electronic states [8]. It is well established that Auger decay of resonantly excited core-hole states in rare gas atoms is often accompanied by anomalously strong shake processes [9,10], so that the same final state may be populated through the decay of different resonances. Electronic state interferences involving a participator Auger decay were indeed observed in resonant Auger spectra of Ne [11]. Since the energy separation of the Ne $1s^{-1}3p$-$4p$ states is large (1.65 eV) compared to the lifetime broadening (0.22 eV), significant interference effects were observed only at excitation energies between the two resonances, where the two intermediate states are excited with comparable strengths. For spectra taken at resonance energies, the interference contribution was negligible.

In this Letter, we report the first observation of interferences induced by *fluorescence decay* of coherently excited core-hole electronic states. The effect is observed in resonant inelastic x-ray scattering (RIXS) on gas-phase hydrogen chloride, HCl. A comprehensive series of high-resolution *KL* RIXS spectra of HCl was recorded, covering the region of the Cl $1s \rightarrow 6\sigma^*$ resonance and the higher lying Rydberg states converging to the Cl *K*-shell ionization threshold. The interferences are revealed by comparing the experimental data with theoretical calculations which include or omit the interference terms. Again, as the energy gap (2.80 eV) between the Cl $(1s)^{-1}6\sigma^*$—the lowest unoccupied molecular orbital (LUMO), and the Cl $(1s)^{-1}4s$, $4p$, $3d$ Rydberg states is considerably larger than the Cl $(1s)^{-1}$ lifetime broadening (0.64 eV [12]), interference effects are expected to show up for excitation energies between the Cl $(1s)^{-1}6\sigma^*$ and the corresponding Rydberg states (Fig. 1). HCl is a target of choice for such studies, because the overlap between the states is significantly enhanced by a dynamical broadening of the dissociative Cl $(1s)^{-1}6\sigma^*$ resonance. In atomic chlorine the overlap is much smaller since the energy difference between the lowest inner-hole atomic state $1s^{-1}3p^6$ and the nearest $1s^{-1}3p^{-1}4p$ group of Rydberg states is estimated to be as much as 11 eV [13]. Argon, the next element in the periodic table, exhibits an energy difference of only 2.46 eV between the lowest core-excited atomic states

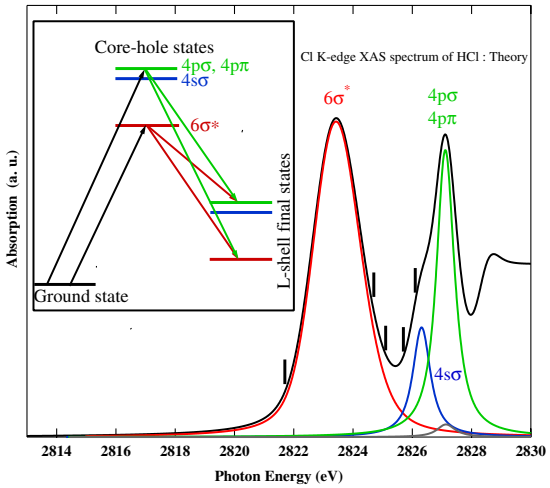

FIG. 1 (color online). Theoretical absorption spectrum of HCl around the Cl K edge. Vertical bars indicate the excitation energies of the spectra presented in Fig. 3. The inset shows two pairs of interfering paths leading to the same final state through the core-excited $6\sigma^*$ state and a group of Rydberg states.

$1s^{-1}4p - 5p^1P_1$ [14], and the overlap is relatively large, but due to strong Rydberg character of the electronic valence states, the participator KL fluorescence transitions are expected to be very weak.

From an experimental point of view, it is challenging to record a full (ω_1, ω_2) RIXS spectral map of a gaseous target with both high resolution and high statistics. In this study, the emission energy ω_2 covers the energy region of Cl KL emission lines, and the incoming photon energy ω_1 scans the Cl K-hole threshold region, which also includes off-resonance excitation energies (large energy detunings) and consequently very low RIXS cross sections. As in our recent RIXS study of doubly excited atomic states [15], the detection efficiency is increased by combining a position sensitive detection with off-Rowland-circle geometry. Experiments were done at the ID26 beamline of the European Synchrotron Radiation Facility (ESRF). The beam line is equipped with a cryogenically cooled double Si(111) crystal monochromator with 0.45 eV bandpass at the energy of the Cl K absorption edge (2830 eV). Incident flux on the target was $\sim 5 \times 10^{12}$ photons/s, and the beam cross section was 200×50 μm^2. A stainless-steel gas cell was filled with 170 mbar of HCl gas and separated from the spectrometer vacuum chamber with 12.5 μm thick polyimide film. First order reflection of a Si(111) crystal was used together with position sensitive detection of photons on a thermoelectrically cooled CCD camera ($-40\,^\circ$C, 22.5×22.5 μm^2 pixel size) to simultaneously measure the whole KL RIXS spectrum at a fixed detector position. The emission was observed along the horizontal polarization of the incident photon beam. The target cell was positioned inside the Rowland circle at a distance of 27 cm in front of the diffraction crystal. Such a geometry enables the collection of fluorescence from a target length of few mm without loss of spectrometer energy resolution with respect to the point source (0.45 at 2620 eV). A total of 101 spectra were recorded, each at a different incident photon energy. The acquisition time for each spectrum was 120 seconds and ω_1 was tuned across the Cl K edge, ranging from 2815 to 2835 eV with 0.20 eV step size. The whole set of measured RIXS spectra was stacked to compose the (ω_1, ω_2) spectral map, which is presented in Fig. 2(a).

The measured RIXS map exhibits two distinct types of behavior. The strong signal observed below 2825 eV corresponds to the promotion of a Cl $1s$ electron to the $6\sigma^*$ LUMO. While a complete breakdown of linear dispersion is noted throughout the resonance region, the linearity is gradually restored at large energy detunings when the excitation energy is moved away from the resonance energy. Such a behavior has been predicted [16], and experimentally observed [17]. It can be qualitatively described using the concept of effective scattering duration time, $\tau^{-1} = \sqrt{\Omega^2 + \Gamma^2}$, which is shortened when the energy detuning Ω is increased. Because of the dissociative character of $(1s)^{-1}6\sigma^*$ resonance, a part of the excitation energy can be transferred into nuclear motion when the scattering lasts long enough. This leads to a broadening of the $\mathrm{Cl}(1s)^{-1}6\sigma^* \rightarrow \mathrm{Cl}(2p)^{-1}6\sigma^*$ emission lines at large energy detunings, an effect absent in the decay of the Rydberg states. For excitation energies above 2825 eV the signal corresponds to the promotion of the Cl $1s$ core electron to the $4s\sigma$ and $4p\sigma$, π Rydberg states. For these states the emission lines show a perfect linear dispersion, a

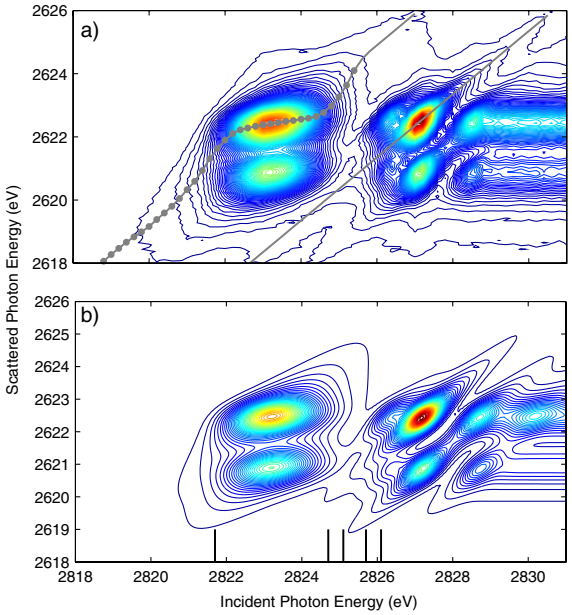

FIG. 2 (color online). Experimental (top) and theoretical (bottom) two-dimensional RIXS KL emission diagrams for HCl around the Cl K edge. Gray lines in (a) indicate position of the maximum of the $(1s)^{-1}6\sigma^* \rightarrow (2p_{3/2})^{-1}6\sigma^*$ (gray dots) and $(1s)^{-1}4\pi$, $\sigma \rightarrow (2p_{3/2})^{-1}4\pi$, σ emission lines as a function of excitation energy. Vertical solid lines in (b) indicate the selected excitation energies used for comparison in Fig. 3.

characteristic feature of atomic resonant Raman x-ray scattering.

The complete RIXS map measured with high-energy resolution provides a unique opportunity to thoroughly test the calculated potential energy surfaces (PES) of the initial (ground state) and valence intermediate $(1s)^{-1}\mathcal{V}$ and final $(2p)^{-1}\mathcal{V}$ states. In this work, PES calculated along the H-Cl bond were fitted with a Morse potential for the ground state [18], or computed at a post Hartree-Fock (HF) theory level for the intermediate and final states, using configuration interaction (CI) with augmented correlation-consistent polarized valence quadruple-zeta basis set *aug-cc-pCVQZ* and *aug-cc-pVQZ* for chlorine and hydrogen, respectively. For the intermediate states, the total number of correlated orbitals derived from the core-hole state wave function included in the CI active space consists of the five outermost doubly occupied H-Cl molecular orbitals, the Cl 1*s* inner-shell, and the 50 lowest unoccupied valence-Rydberg virtual orbitals. For each PES, vibrational wave functions were calculated using a one-dimensional Hamiltonian model as described in Ref. [19]. Relaxation of valence orbitals in response to the core-hole formation has been taken into account by using HF-SCF orbitals, optimized for Cl $(2s)^{-1}6\sigma^*$ intermediate state. Choosing the orthogonal orbital set based on Cl 2*s* instead of Cl 1*s* hole allows to obtain a ground state wave function of comparable quality as given by the single SCF determinant for the ground state [20]. A partial recovery of the overall relaxation of the valence-shells in this case is compensated by more accurate values of transition moments along the H-Cl bond coordinate (calculated in the dipole-length form). For transitions below the ionization threshold, variations of the vibrational and the electronic parts of the transition moment along the inter atomic bond distances were integrated simultaneously.

Because of spin-orbit (SO) coupling, the $(2p)^{-1}\mathcal{V}$ final states are linear combinations of triplet and singlet nonrelativistic components. In addition to the $(2p)^{-1}\sigma^*$ SO states, already reported in [19,21], the Rydberg $(2p)^{-1}\mathcal{R}$ spin-orbit states were fully calculated *ab initio* for HCl at equilibrium bond length (1.28 Å). The integral package in GAMESS(US) [22] with all Breit-Pauli coupling terms [23–25] was used for calculations of the 2*p* core-excited states. The $2p \rightarrow 1s$ oscillator strength is given by the transition probability between the localized Cl 1*s* and the nonrelativistic singlet $^1\Sigma^+$ or degenerate $^1\Pi$ 2*p* components, multiplied by the weights (populations) of these states in the relativistic configuration.

The final result of our calculations is presented in Fig. 2(b) and shows an excellent agreement with the experimental data [Fig. 2(a)]. However, to reproduce accurately the measured RIXS spectra at all excitation energies, interference terms need to be included in the calculations, as demonstrated in Fig. 3 by a detailed comparison of emission spectra recorded at selected excitation energies. The effect is described in terms of doubly differential cross section (DDCS), which determines the spectral properties of resonant x-ray scattering [26]. For a long-lived final state, the DDCS is given by

$$\frac{d^2\sigma}{d\omega_1 d\omega_2} = \sum_f |F_f(\omega_1, \vec{e}_1, \vec{e}_2)|^2 \delta(\omega_1 - \omega_2 - \omega_{fo}), \quad (1)$$

where $\vec{e}_1$ and $\vec{e}_2$ are polarization vectors of the incoming and emitted photon, respectively, and the summation runs over the available final states. The transition energy from the ground state to the final $(2p)^{-1}\mathcal{V}$ state is denoted by ω_{fo}. For *KL* decay in HCl the final state has an empty $2p_{1/2}$ or $2p_{3/2}$ orbital and one electron occupies $6\sigma^*$ or Rydberg-like molecular orbital. The diffusion factors are given by coherent summation of absorption-emission amplitudes over all allowed intermediate states $|i\rangle$, which take the system from the ground state $|o\rangle$ to the final state $|f\rangle$,

$$\begin{aligned} F_f &= \sum_i \frac{\langle f|\hat{\mathcal{D}}|i\rangle\langle i|\hat{\mathcal{D}}|o\rangle}{\omega_1 - \omega_{io} + \imath\Gamma/2} \\ &= \frac{\langle f|\hat{\mathcal{D}}|1s^{-1}6\sigma^*\rangle\langle 1s^{-1}6\sigma^*|\hat{\mathcal{D}}|o\rangle}{\omega_1 - \omega_{6\sigma^*} + \imath\Gamma/2} \\ &\quad + \sum_{\mathcal{R}} \frac{\langle f|\hat{\mathcal{D}}|1s^{-1}\mathcal{R}\rangle\langle 1s^{-1}\mathcal{R}|\hat{\mathcal{D}}|o\rangle}{\omega_1 - \omega_{\mathcal{R}} + \imath\Gamma/2}. \end{aligned} \quad (2)$$

Here, the final states are $(2p)^{-1}6\sigma^*$ or any of the $(2p)^{-1}\mathcal{R}$ states, and the sum runs over $(1s)^{-1}6\sigma^*$ and $(1s)^{-1}\mathcal{R}/\mathcal{C}$ Rydberg or continuum intermediate states. $\hat{\mathcal{D}}$ represents

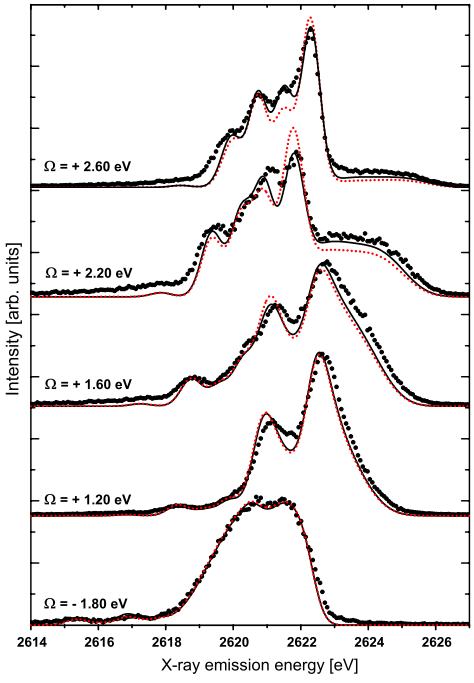

FIG. 3 (color online). Experimental *KL* emission spectra of HCl at selected excitation energies (see Figs. 1 and 2), compared to calculated spectra with (full line) and without (dotted line) the electronic state interference terms. Ω denotes the detuning from the $(1s)^{-1}6\sigma^*$ resonance energy.

the dipole transition operator and Γ denotes the lifetime broadening of the Cl $1s$ hole. The excitation energies of intermediate states are denoted by ω_{io}. To take into account realistic experimental conditions, the calculated spectra are convoluted by the incident photon beam profile and the spectrometer transmission function, each represented by a Gaussian with 0.45 eV FWHM. The calculation shows that both types of spectator-participator cross terms,

$$|o\rangle \rightarrow (1s)^{-1}6\sigma^* \rightarrow (2p)^{-1}6\sigma^* \text{ spectator,}$$

$$|o\rangle \rightarrow (1s)^{-1}6\sigma^* \rightarrow \sum(2p)^{-1}\mathcal{R} \text{ shakeup,}$$

and

$$|o\rangle \rightarrow \sum(1s)^{-1}\mathcal{R} \rightarrow \sum(2p)^{-1}\mathcal{R} \text{ spectator,}$$

$$|o\rangle \rightarrow \sum(1s)^{-1}\mathcal{R} \rightarrow (2p)^{-1}6\sigma^* \text{ shakedown,}$$

are responsible for the interferences observed in our spectra (see inset in Fig. 1). Although the relative ratio of the participator dipole moments with respect to the spectator transition dipole moments is only about 1:100, the participator terms can still contribute significantly to the RIXS cross section at excitation energies between the $1s \rightarrow 6\sigma^*$ resonance and the Rydberg states (Fig. 3). On the other hand, to reproduce spectra measured at small energy detunings, interference terms may be neglected because the spectator amplitude dominates over the amplitude of the weakly excited participator decay channel.

In conclusion, the KL spectral map of inelastically scattered x rays in the region of Cl K edge in the HCl molecule was measured with high resolution and compared to fully *ab-initio* calculated spectra. In order to obtain a good agreement between the theoretical and experimental sequence of emission spectra it is necessary to account for the electronic state interferences. The interference effects in RIXS spectra are most strongly exposed at inter resonance excitation energies where coherent excitation of neighboring states occurs with comparable strengths. For weakly overlapping states such an approach requires high experimental sensitivity to measure weak emission signal in the gap between resonances, but this offers a possibility to test with high precision the set of calculated transition amplitudes including their relative phases—the goal of a complete quantum-mechanical measurement.

This work was supported by the Slovenian research program P1-0112. We gratefully acknowledge an excellent assistance of the ID26 beam line staff in preparation of the experiment.

[1] Y. Morioka, T. Aoto, and H. Yoshii, Phys. Rev. A **64**, 053409 (2001).
[2] M. Alagia *et al.*, Phys. Rev. Lett. **102**, 153001 (2009).
[3] T. X. Carroll *et al.*, Phys. Rev. Lett. **58**, 867 (1987).
[4] P. Glans *et al.*, J. Phys. B **26**, 663 (1993).
[5] T. D. Thomas and T. X. Caroll, Chem. Phys. Lett. **185**, 31 (1991).
[6] M. Neeb *et al.*, J. Electron Spectrosc. Relat. Phenom. **67**, 261 (1994).
[7] P. Skytt *et al.*, Phys. Rev. A **55**, 146 (1997).
[8] A. Cesar and H. Ågren, Phys. Rev. A **45**, 2833 (1992).
[9] H. Aksela *et al.*, Phys. Scr. **41**, 425 (1990).
[10] M. Meyer *et al.*, Phys. Rev. A **43**, 177 (1991).
[11] J.-E Rubensson *et al.*, Chem. Phys. Lett. **257**, 447 (1996).
[12] J. A. Campbell, At. Data Nucl. Data Tables **77**, 1 (2001).
[13] K. G. Dyall *et al.*, Comput. Phys. Commun. **55**, 425 (1989).
[14] M. Breinig *et al.*, Phys. Rev. A **22**, 520 (1980).
[15] M. Kavčič *et al.*, Phys. Rev. Lett. **102**, 143001 (2009).
[16] F. Gel'mukhanov and H. Ågren, Phys. Rep. **312**, 87 (1999).
[17] M. Simon *et al.*, Phys. Rev. A **73**, 020706(R) (2006).
[18] We have used the formula $D_e[1 - e^{-\beta(R-R_0)}]^2$ with parameters $D_e = 4.430$ eV, $\beta = 3.588$ Å^{-1}, $R_0(\mathrm{HCl}) = 1.274$ Å. The Buckingham potential is defined by $E(R) - E(\infty) = A\exp(-\alpha R) - B/R^6$.
[19] R. Guillemin *et al.*, Phys. Rev. Lett. **101**, 133003 (2008).
[20] G. Fronzoni *et al.*, Chem. Phys. **232**, 9 (1998).
[21] S. Carniato *et al.*, Phys. Rev. A **80**, 032513 (2009).
[22] M. W. Schmidt *et al.*, J. Comput. Chem. **14**, 1347 (1993).
[23] T. R. Furlani, H. F. King, J. Chem. Phys. **82**, 5577 (1985).
[24] H. F. King, T. R. Furlani, J. Comput. Chem. **9**, 771 (1988).
[25] D. G. Fedorov, M. S. Gordon, J. Chem. Phys. **112**, 5611 (2000).
[26] J. J. Sakurai, *Advanced Quantum Mechanics* (Addison-Wesley, New York, 1967).